STUDY ON PREDICTION EQUATIONS OF STATISTICAL VALUES OF GROUP DELAY TIME USING GROUND MOTION PARAMETERS

K. Nagao(1), Y. Nakamura(2)

(1) *Structural Engineer, Daiwa House Industry, nagaok@daiwahouse.jp*
(2) *Associate Professor, Chiba University, nakamura.yukiko@faculty.chiba-u.jp*

Abstract

Some non-linear responses of structures, such as cumulative damages, are mainly influenced by non-stationary characteristics of artificial ground motion, such as the duration of strong motion. Hence, it is necessary to appropriately evaluate the non-stationary characteristics of the ground motions expected in construction sites. Previous studies have mathematically proven that the group delay time plays a key role in defining the non-stationary characteristics of artificial ground motions. Furthermore, the values of mean and standard deviation of the group delay time (μ_{tgr} and σ_{tgr}, respectively) are considered as the mean arrival time and the duration of strong motion of the phase wave, respectively. In this study, μ_{tgr} and σ_{tgr} were computed in 1.0-Hz-width and 0.15-Hz-width frequency bands using acceleration records (horizontal and vertical components) of 15 crustal earthquakes in the KiK-net (Kiban-Kyoshin net) and NGA (Next Generation of Ground-Motion Attenuation Models) West2 databases. Additionally, the relationships between μ_{tgr} and σ_{tgr} and ground motion parameters such as the moment magnitude (M_w), closest source-to-site-distance (R_{rup}), shallow soil property (V_{s30}, the average shear wave velocity in the top 30 m), deep soil property ($Z_{1.0}$, depth to layer at shear wave velocity exceeds 1.0 km/s), and forward directivity effect were investigated.

Multiple regression analyses revealed the increasing tendency of μ_{tgr} and σ_{tgr} (i.e. the delay of the mean arrival times and elongation of the durations of strong motion) with the increase in M_w and R_{rup} in nearly all frequency bands. On the other hand, residual analyses indicated that the shallow and deep soil properties mainly influence μ_{tgr} and σ_{tgr} in low frequency bands (up to approximately 2.0 Hz). As the value of V_{s30} decreased, the values of μ_{tgr} and σ_{tgr} increased. Due to the strong shaking, soils with low values of V_{s30} could vibrate non-linearly, thereby resulting in a delay of the mean arrival times and elongation of the durations of strong motion. On the other hand, as the value of $Z_{1.0}$ increased, μ_{tgr} and σ_{tgr} increased. The surface wave produced by the basin effects might cause the delay of the mean arrival times and elongation of the durations of strong motion for the soils with high values of $Z_{1.0}$. The forward directivity effect on μ_{tgr} and σ_{tgr} was investigated by comparing the values of μ_{tgr} and σ_{tgr} for pulse-like ground motions with those for non-pulse-like ground motions. The comparisons revealed that the pulse-like ground motions tend to have lower values of σ_{tgr} than the non-pulse-like ground motions (up to 3.0 Hz). Furthermore, for pulse-like ground motions, it was observed that the values of μ_{tgr} and σ_{tgr} tend to decrease as R_{rup} decreases.

Finally, regression analyses were performed, and the regression coefficients for M_w, R_{rup}, V_{s30}, $Z_{1.0}$, and the forward directivity effect were presented. Additionally, the effect of each paramter was discussed by comparing the predicted values.

Keywords: group delay time, shear wave velocity, basin effect, forward directivity

1. Introduction

Dynamic analyses using design artificial ground motions is required when designing high rise buildings or buildings equipped with energy dissipation devices or base-isolation systems. In Japan, artificial ground motions are developed using 1) phase angles of common recorded ground motions, 2) random phase angles, and 3) elaborate fault models. In methods 1) and 2), the expected earthquake parameters for each construction site (earthquake magnitude, distance from the source to site, and local site conditions) are not considered.

Contrarily, detailed information regarding the fault geometry, path, and site conditions is considered in the third method. However, the third method is usually costly and time-consming.

On the other hand, Ohsaki [1] and Izumi and Katsukura [2] pointed out that the histograms of the group delay time (t_{gr}) of ground motions have shapes that are similar to the envelopes of ground motions. Furthermore, these similarities were mathematically proven based on the physical meanings of t_{gr} [3]. Therefore, the values of the mean and the standard deviation of the group delay time (denoted as μ_{tgr} and σ_{tgr}, respectively) can be considered as the mean arrival time and the duration of strong motion of the phase wave, respectively. Moreover, a positive correlation was observed between μ_{tgr} and σ_{tgr} [4]. Because of the relationship between non-stationary characteristics and t_{gr} of ground motion, the values of μ_{tgr} and σ_{tgr} can be influenced by the source, path, and site conditions of an earthquake. These parameters were used to develop empirical equations for the durations of strong motion (e.g., the time interval between 5–95 % of the Arias intensity) [5-8]. On the other hand, the response spectra are mainly influenced by μ_{tgr}. For example, component waves with the same mean arrival time could amplify the peak responses via the interference effect, thereby resulting in large response spectra. Thus, the non-stationary characteristics of natural ground motions may not be incorporated in design artificial ground motions by only accounting for the duration characteristics.

In this study, the values of μ_{tgr} and σ_{tgr} were computed using 997 acceleration records (two horizontal and vertical components) of 15 crustal earthquakes in the KiK-net (Kiban-Kyoshin net) and NGA (Next Generation of Ground-Motion Attenuation Models) West2 databases. To investigate the non-stationary characteristics of component waves in different frequencies, the values of μ_{tgr} and σ_{tgr} were computed in 1.0-Hz-width and 0.15-Hz-width frequency bands. Additionally, the relationships between μ_{tgr} and σ_{tgr} and the moment magnitude (M_w), closest source-to-site-distance (R_{rup}), shallow soil property (V_{s30}, the average shear wave velocity in the top 30 m) , deep soil property ($Z_{1.0}$, depth to layer at shear wave velocity becomes more than 1.0 km/s), and forward directivity effect were investigated. Finally, the regression models for μ_{tgr} and σ_{tgr} were constructed using the abovementioned ground motion parameters, and the regression coefficients were presented. Furthemore, the effect of each parameter was discussed by comparing the predicted models.

2. Ground motion data set and definition of group delay time

2.1 Ground motion dataset

The acceleration records (two horizontal and vertical components) from 15 crustal earthquakes were used; the details of the earthquakes are listed in Table 1. It should be noted that records with epicentral distances less than 200 km were used. All ground motions were set such that their P-wave appeared from 0 s. In addition, all ground motions were zero-padded such that the sample size was 131072. Furthermore, the time step was 0.01 s. Thus, the record length T was 1310.72 s.

Table 1 – Details of 15 crustal earthquakes

No	Name	M_w	Hypocenter	Date	# of records	Data
1	Tottoriken seibu	6.7	long:133.35 lat:35.28	2000/10/6	72	KiK
2	Niigataken chuetsu	6.6	long:138.87 lat:37.29	2004/10/23	133	KiK
3	Fukuokaken seihouoki	6.6	long:130.18 lat:33.74	2005/3/20	75	KiK
4	Notohanto oki	6.7	long:136.69 lat:37.22	2007/3/25	66	KiK
5	Niigataken chuetsuoki	6.6	long:138.61 lat:37.56	2007/7/16	124	KiK
6	Iwate miyagi nairiku	6.9	long:140.88 lat:39.00	2008/6/14	97	KiK
7	Naganoken hokubu	6.3	long:138.60 lat:36.98	2011/3/12	141	KiK
8	Fukushimaken hamadori	6.7	long:140.67 lat:36.95	2011/4/11	88	KiK
9	Kumamoto	7.0	long:130.76 lat:32.75	2016/4/16	77	KiK
10	Landers	7.3	long:-116.44 lat:34.20	1992/6/28	11	NGA
11	Kobe	6.9	long:135.01 lat:34.60	1995/1/16	14	NGA
12	Chi-Chi	7.6	long:120.82 lat:23.85	1999/9/20	14	NGA
13	Hector Mine	7.1	long:-116.26 lat:34.60	1999/10/16	22	NGA
14	San Simeon	6.5	long:-121.09 lat:35.70	2003/12/22	7	NGA
15	El Mayor-Cucapah	7.2	long:-115.27 lat:32.30	2010/4/4	56	NGA

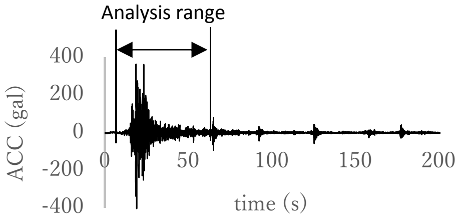

Fig. 1 – Example of analysis range

2.2 Definition of group delay time

The k^{th} group delay time $t_{gr,k}$ is defined as follows:

$$t_{gr,k} = \Delta\phi_k / \Delta\omega \quad (1)$$

$$\Delta\phi_k = \phi_{k+1} - \phi_k \quad (2)$$

$$\phi_k = \tan^{-1}\frac{-B_k}{A_k} \quad (3)$$

where $\Delta\phi_k$ is the k^{th} phase difference (rad) [1], ϕ_k is the k^{th} phase angle (rad), $\Delta\omega$ is the increment of signal circular frequency (rad/s), and A_k and B_k are the real and imaginary parts, respectively, of the Fourier complex numbers. All values of $t_{gr,k}$ and $\Delta\phi_k$ were defined within the ranges of [0, -T] and [0, -2π], respectively.

The values of mean and standard deviation of group delay time (μ_{tgr} and σ_{tgr}) were computed in the following two types of narrow frequency bands:

0.10–1.0 Hz, 1.0–2.0 Hz, 2.0–3.0 Hz, …, 8.0–9.0 Hz, 9.0–10.0 Hz (denoted as *fb*1–*fb*10)

0.10–0.25 Hz, 0.25–0.40 Hz, …, 0.70–0.85 Hz, 0.85–1.0 Hz (denoted as *fb*1a–*fb*1f)

If the width of the frequency band is excessively narrow, the values of σ_{tgr} become unstable. However, if the width is significantly broad, detailed information of the non-stationary characteristics in long period ranges cannot be obtained. In this study, it was confirmed that the correlation coefficient between the values of σ_{tgr} in the two orthogonal components exceeded 0.50 when using the 0.15-Hz-width frequency band. Thus, it was considered that the 0.15-Hz-width was sufficiently broad for obtaining stabilized values of σ_{tgr}.

The values of μ_{tgr} and σ_{tgr} were computed for all components, (i.e., two horizontal and one vertical component) using the following steps. Thereafter, μ_{tgr} and σ_{tgr} for the two horizontal components were averaged. Steps 1–4 were performed within each of the sixteen narrow frequency bands.

1. Compute the mean value of t_{gr}.
2. Add T to the values of t_{gr} that are less than the mean value minus T/2. Additionally, subtract T from the values of t_{gr} that exceed the mean value plus T/2.
3. Compute the values of the mean and standard deviation of t_{gr}.
4. Eliminate t_{gr} outside the mean±4 standard deviation (referred to as outliers), then go back to Step 2. After all the values of t_{gr} are within mean±4 standard deviation, the values of the mean and standard deviation of t_{gr} are set as μ_{tgr} and σ_{tgr}, respectively.

While outliers can significantly influence the statistical values of t_{gr}, Nagao and Kanda [9] demonstrated that the Fourier amplitudes are significantly small at frequencies where t_{gr} exceeds the mean±4 standard deviation limit. Hereafter, the subscript h and v are added to represent the horizontal component and the vertical component, respectively.

The small tremors following strong motions might cause an overestimation of σ_{tgr}. To avoid this overestimation, the analysis ranges were set to exclude such tremors. See Fig.1, for example. On the other hand, in some ground motions of the NGA West2 database, the amplitudes at the end of the records did not converge to zero due to the long surface wave, which causes the underestimation of σ_{tgr} in low frequency bands. Thus, ground motions whose record length were less than $\mu_{tgr,0.1\text{-}1.0}$ + 2 $\sigma_{tgr,0.1\text{-}1.0}$ (μ_{tgr} and σ_{tgr} calculated in 0.10–1.0 Hz) were not considered in this study.

3. Development of empirical equations

3.1 Base model

Empirical models for μ_{tgr} and σ_{tgr} are developed by accounting for the source and path parameters. It should be noted that the rupture time tends to increase as the value of M_w increases. Thus, it can be argued that the rupture time and M_w have positive correlations. Kempton and Stewart [6] developed empirical models for the durations of strong motions using the inverse of the corner frequency as the source parameter, which represents the source duration and is also a function of the seismic moment and stress drop. The models developed by

Kempton and Stewart were based on a theoretical background; however, Nojima [8] developed simplified models by using M_w as the only source parameter. Furthermore, it was pointed out that the models proposed by Nojima and those proposed by Kempton and Stewart yielded similar predicted values, which validates the use of only M_w for simplicity [8].

On the other hand, as the distance from the source increases, the seismic wave in the time domain spreads. Various types of distances were used for the empirical models for durations including the epicentral distance, hypocentral distance, and R_{rup}. To account for the source dimension, R_{rup} was used in this study.

The values of μ_{tgr} and σ_{tgr} are positive. Additionally, the differences between the observed and predicted values could increase as the predicted values increase. Thus, the following equation was used to consider the effects of the source and path parameters.

$$\ln \mu_{tgr}(\ln \sigma_{tgr}) = mM_w + r \ln(R_{rup} + h) + c \tag{4}$$

where m, r, h, and c are the regression coefficients.

The coefficient h was used to avoid the divergence of $\ln(R_{rup})$ when R_{rup} takes values close to 0 km. In previous studies [6, 7], the values of h ranged from 2.0–46 km. In this study, the values of h were determined using the following calculations: the values of $\mu_{tgr,h}$, $\sigma_{tgr,h}$, $\mu_{tgr,v}$, and $\sigma_{tgr,v}$ in *fb*1–*fb*10 were averaged to obtain $\mu_{tgr,h,0.1\text{-}10.0}$, $\sigma_{tgr,h,0.1\text{-}10.0}$, $\mu_{tgr,v,0.1\text{-}10.0}$, and $\sigma_{tgr,v,0.1\text{-}10.0}$, respectively. Thereafter, the value of h with the highest correlation coefficient was investigated within the range of h = 0–100 km for each of $\mu_{tgr,h,0.1\text{-}10.0}$, $\sigma_{tgr,h,0.1\text{-}10.0}$, $\mu_{tgr,v,0.1\text{-}10.0}$, and $\sigma_{tgr,v,0.1\text{-}10.0}$; the optimum values of h were found to be 53 km, 100 km, 32 km, 27 km, respectively. By comparing the optimum values of h with the values of h reported by previous studies, h was set as 32 km for $\mu_{tgr,h}$ and $\mu_{tgr,v}$ and 27 km for $\sigma_{tgr,h}$ and $\sigma_{tgr,v}$. The optimum values of h were also investigated in the sixteen narrow frequency bands. However, in approximately half of the narrow frequency bands, the optimum value of h was either 0 km or 100 km.

3.2 Effect of shallow soil property

The effects of shallow soil properties represented by V_{s30} are investigated. It should be noted that the values of V_{s30} (as well as $Z_{1.0}$) for KiK net sites were obtained using PS logging data. First, the predicted values of $\mu_{tgr,h}$, $\mu_{tgr,v}$, $\sigma_{tgr,h}$, and $\sigma_{tgr,v}$ were computed using Eq. (4). Subsequently, residuals ε_1 defined by the observed value minus the predicted value were computed. The relationship between ε_1 and ln V_{s30} for $\sigma_{tgr,h}$ are shown in Fig.2. The linear regression line is superimposed in each subplot.

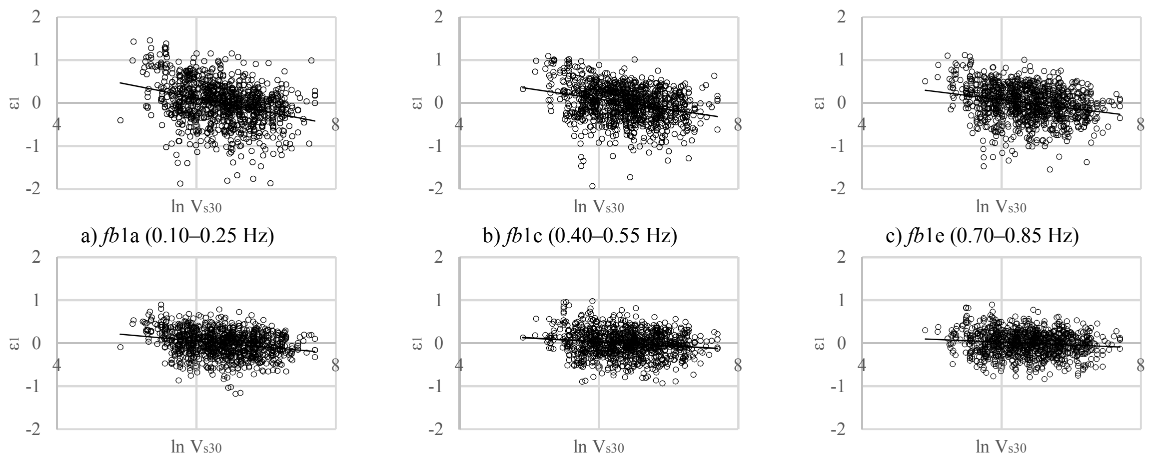

a) *fb*1a (0.10–0.25 Hz) b) *fb*1c (0.40–0.55 Hz) c) *fb*1e (0.70–0.85 Hz)

d) *fb*2 (1.0–2.0 Hz), e) *fb*4 (3.0–4.0 Hz) f) *fb*6 (5.0–6.0 Hz)

Fig. 2 – Relationships between residual (ε_1) and ln V_{s30} for $\sigma_{tgr,h}$

Figs.2 a–d shows the tendency of ε_1 to decrease from positive values to negative values as ln V_{s30} increases in *fb*1a–*fb*2. Soils with a low value of V_{s30} might have long natural periods. During the strong and long-period shaking, soft soils might vibrate nonlinearly due to the resonant effect. As a result, the duration of strong motion in the long period range may be lengthened. On the other hand, as shown in Figs.2 d–e, V_{s30} exerted minor effects on $\sigma_{tgr,h}$ in high frequency bands. Soils with a high V_{s30} tend to have short natural periods and high material damping, which might reduce the short-period ground motion. The relationship between ε_1 and ln V_{s30} for $\mu_{tgr,h}$ was also investigated; this is depicted in Fig.3. The same tendency as $\sigma_{tgr,h}$ was observed in low frequency bands, where ε_1 decreases from positive values to negative values as ln V_{s30} increases, whereas V_{s30} has a relatively weak correlation with ε_1 in high frequency bands.

Based on the abovementioned discussion, the residuals ε_1 were modeled using the following equation:

$$\varepsilon_1 = v_1 + v_2 \ln V_{s30} \tag{5}$$

where v_1 and v_2 are the regression coefficients. Furthermore, it was confirmed that higher correlation coefficients were obtained when using ln V_{s30}, as compared to when using V_{s30}.

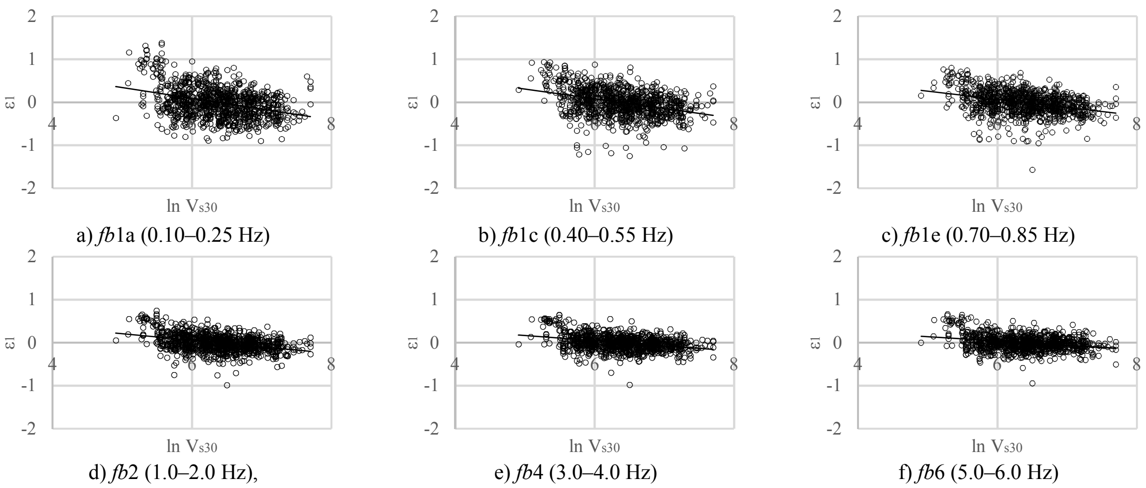

Fig. 3 – Relationships between residual (ε_1) and ln V_{s30} for $\mu_{tgr,h}$

3.3 Effect of deep soil property

The effects of deep soil properties represented by $Z_{1.0}$ are investigated. While V_{s30} can be obtained relatively easily, $Z_{1.0}$ is not always available, especially when the sedimentary layer is thick at construction sites. However, the value of $Z_{1.0}$ is correlated with the value of V_{s30} [10-12]. The relationships between $Z_{1.0}$ and V_{s30} in Japanese sites and other sites (including American, Mexican, and Taiwanese sites) are shown in Fig.4. Furthermore, the regression lines defined by the following equations are superimposed. The functional forms of Eq. (6) were derived from previous studies [10-12].

For Japanese sites:
$$\ln Z_{1.0} = -3.05 \ln\left(\frac{V_{s30}^2+450^2}{1360^2+450^2}\right) \tag{6a}$$

For other sites:
$$\ln Z_{1.0} = -1.45 \ln\left(\frac{V_{s30}^4+335^4}{1360^4+335^4}\right) \tag{6b}$$

In this study, the correlation between $Z_{1.0}$ and V_{s30} influenced the form of the statistical models. In multiple regression analysis, each explanatory coefficient is usually considered to be statistically independent. Thus, the effects of soil properties are represented by the residual terms, which should be added to the values predicted by the base model in Eq. (4).

The effects of $Z_{1.0}$ were evaluated via the following procedure: First, the sum of the values predicted by the base model (Eq. 4) and ε_1 (Eq. 5) were computed. Subsequently, the residual ε_2 was defined as the observed value minus the summed value. The relationships between ε_2 and $Z_{1.0}$ are plotted for $\sigma_{tgr,h}$ and $\mu_{tgr,h}$ as shown in Fig.5 and Fig.6, respectively. Additionally, the regression line is added to each subplot.

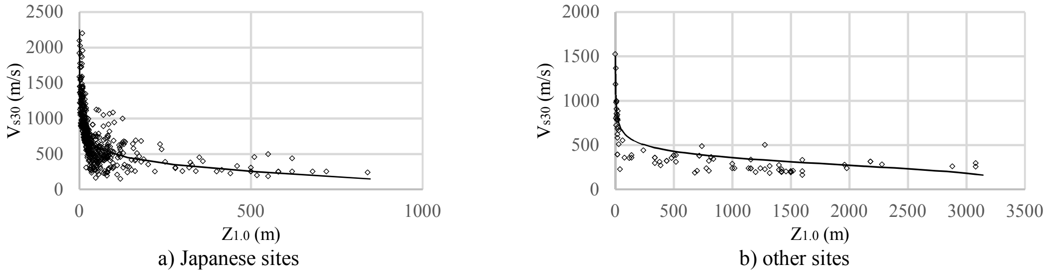

Fig. 4 – Relationships between $Z_{1.0}$ and V_{s30} for a) Japanese sites and b) other sites

From Figs.5 a–d, the tendency for ε_2 to increase as $Z_{1.0}$ increases can be observed. For a large $Z_{1.0}$ (i.e., the sedimentary layer is thick), the surface wave caused by the basin effect can be prominent, causing long durations of strong motions in low frequency ranges. On the contrary, no tendencies can be observed in high frequency bands. Regarding $\mu_{tgr,h}$, the tendency for ε_2 to increase as $Z_{1.0}$ increases can be obtained in all frequency bands. Furthermore, the slopes of the regression lines are larger in low frequency bands.

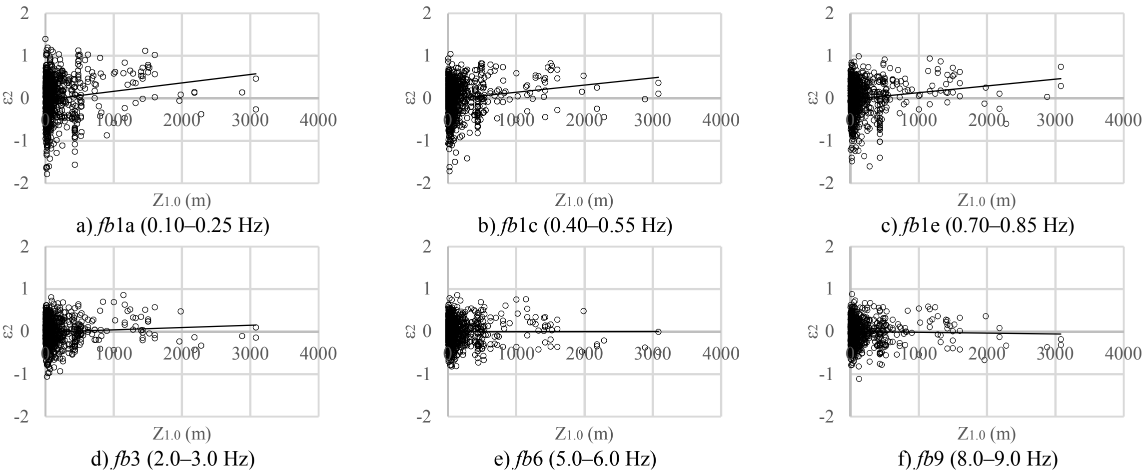

Fig. 5 – Relationships between residual (ε_2) and $Z_{1.0}$ for $\sigma_{tgr,h}$

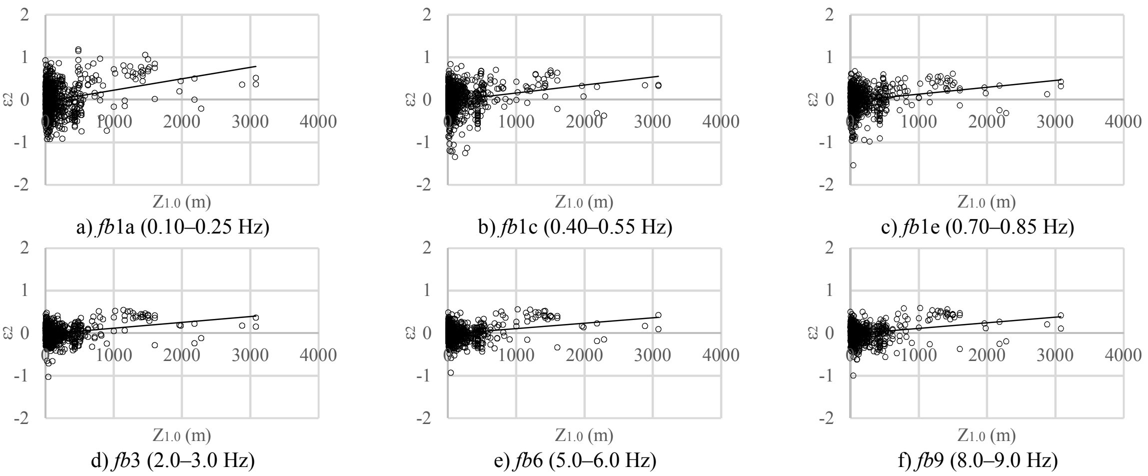

Fig. 6 – Relationships between residual (ε_2) and $Z_{1.0}$ for $\mu_{tgr,h}$

Based on the abovementioned discussion, the residuals ε_2 were modeled using the following equation:

$$\varepsilon_2 = z_1 + z_2 Z_{1.0} \tag{7}$$

where z_1 and z_2 are the regression coefficients. Furthermore, it was confirmed that higher correlation coefficients were obtained when using $Z_{1.0}$, as compared to when using $\ln Z_{1.0}$.

3.4 Effect of forward directivity effect

It was indicated that the forward directivity effect causes a shortening of the durations. Previous studies [6,13] have proposed the modification factor for the durations of ground motions influenced by the forward directivity effect. The durations were computed using broadband records. On the contrary, Sommerville and Smith [13] stated that the differences between the fault-parallel and fault-normal response spectra resulting from the forward directivity effect were observed in periods exceeding 0.5 s. Therefore, the forward directivity effect on the duration of strong motion might depend on frequency.

In this study, the influences of the forward directivity effect are investigated by comparing the values of μ_{tgr} and σ_{tgr} for pulse-like ground motions with those for non-pulse-like ground motions. Shahi and Baker [14] and Hayden [15] classified pulse-like ground motions caused by the forward directivity effect by analyzing ground motions in the NGA West2 database. In this study, acceleration records of earthquakes 10–15 (see Table 1) are from the NGA West2 database. Moreover, some acceleration records for earthquakes 1, 2, 5, and 6 are also included in the NGA West2 database. Thus, the forward directivity effect on μ_{tgr} and σ_{tgr} was investigated by using the data for these ten earthquakes. Hereafter, the pulse-like ground motions and non-pulse-like ground motions are denoted as *P* and *NP*, respectively.

First, the sum of the values predicted by the base model (Eq. 4), predicted residuals ε_1 (Eq. 5), and predicted residuals ε_2 (Eq. 7) were computed. Subsequently, the residual ε_3 was computed as the observed value minus the summed value. The relationships between ε_3 and R_{rup} for $\sigma_{tgr,h}$ are shown in Fig.7. Additionally, a regression line is superimposed for *P*. The relationships between ε_3 and R_{rup} for $\mu_{tgr,h}$ are presented in Fig.8.

As shown in Figs.7 a–d, ε_3 increases as R_{rup} increases for the *P* data, indicating that the observed values of $\sigma_{tgr,h}$ are less than the predicted values of $\sigma_{tgr,h}$ for a small R_{rup}. A relatively weak correlation relationship can be observed between ε_3 and R_{rup} in Figs.7 e–f. Similar trends can be observed in Fig.8. As reported by Sommerville and Smith [13], the forward directivity effect might weaken in high frequency bands.

However, Figs.7 a–c and Figs.8 a–c show that some of the *NP* data for R_{rup} that are less than 10 km also take negative values of ε_3. In Eq. (4), the coefficient h was used to avoid the divergence of $\ln R_{rup}$ when R_{rup} is close to zero. In this study, h was set as 32 km for $\mu_{tgr,h}$ and $\mu_{tgr,v}$ and 27 km for $\sigma_{tgr,h}$ and $\sigma_{tgr,v}$. The modification effect resulting from h might be more significant for a small R_{rup}. Thus, the predicted values of μ_{tgr} and σ_{tgr} can also be overestimated for *NP* data when R_{rup} is small. To evaluate the difference between ε_3 for *P* and *NP*, the slopes of the regression lines (d_1) in Eq. (8) were compared in Table 2. Moreover, the relationship between ε_3 and R_{rup} was modeled using Eq. (9) for $\mu_{tgr,h}$. The regression coefficients d_2 and d_3 are shown in Table 3. The regression coefficients d_1, d_2, and d_3 were determined by using ε_3 with a value of R_{rup} less than 26.55 km, which is the maximum R_{rup} for *P*.

For $\sigma_{tgr,h}$:
$$\varepsilon_3 = d_1\left(R_{rup} - 26.55\right) \tag{8}$$

For $\mu_{gr,h}$:
$$\varepsilon_3 = d_2 R_{rup} + d_3 \tag{9}$$

Table 2 – Values of d_1 for pulse-like (*P*) and non-pulse-like (*NP*) ground motions

	*fb*1a	*fb*1b	*fb*1c	*fb*1d	*fb*1e	*fb*1f	*fb*1	*fb*2
P	0.0322	0.0495	0.0472	0.0468	0.0391	0.0323	0.0409	0.0166
NP	0.0061	0.0009	0.0101	0.0102	0.0137	0.0086	0.0084	-0.0015

Table 3 – Values of d_2 and d_3 for pulse-like (P) and non-pulse-like (NP) ground motions

		*fb*1a	*fb*1b	*fb*1c	*fb*1d	*fb*1e	*fb*1f	*fb*1	*fb*2
P	d_2	0.0389	0.0478	0.0455	0.0381	0.0331	0.0375	0.0404	0.0268
	d_3	-0.6379	-0.9591	-0.9110	-0.7567	-0.6881	-0.6458	-0.7809	-0.4237
NP	d_2	0.0238	0.0229	0.0286	0.0168	0.0186	0.0070	0.0207	0.0033
	d_3	-0.4415	-0.4387	-0.6243	-0.3780	-0.4099	-0.1901	-0.4319	-0.0882

As shown in Table 2, the values of d_1 for P are greater than those for NP in all frequency bands. Hence, compared to non-pulse-like ground motions, the observed values of $\sigma_{tgr,h}$ for pulse-like ground motions are smaller for the same value of R_{rup} less than 26.55 km. On the other hand, Table 3 indicates that the values of d_3 for P are smaller than the values of d_3 for NP. Compared to non-pulse-like ground motions, the observed values of $\mu_{tgr,h}$ for pulse-like ground motions are smaller for a small R_{rup}.

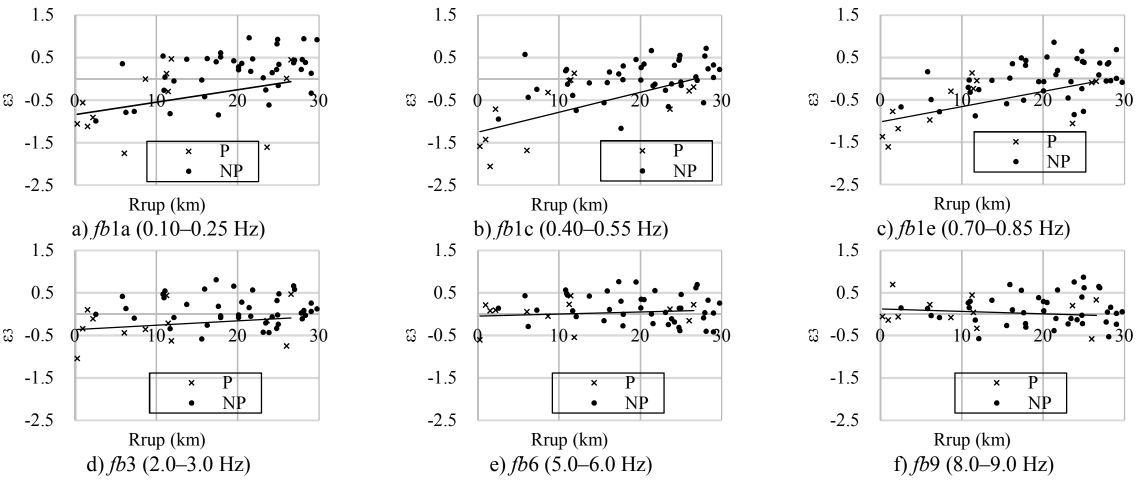

Fig. 7 – Relationships between residual (ε_3) and R_{rup} for $\sigma_{tgr,h}$

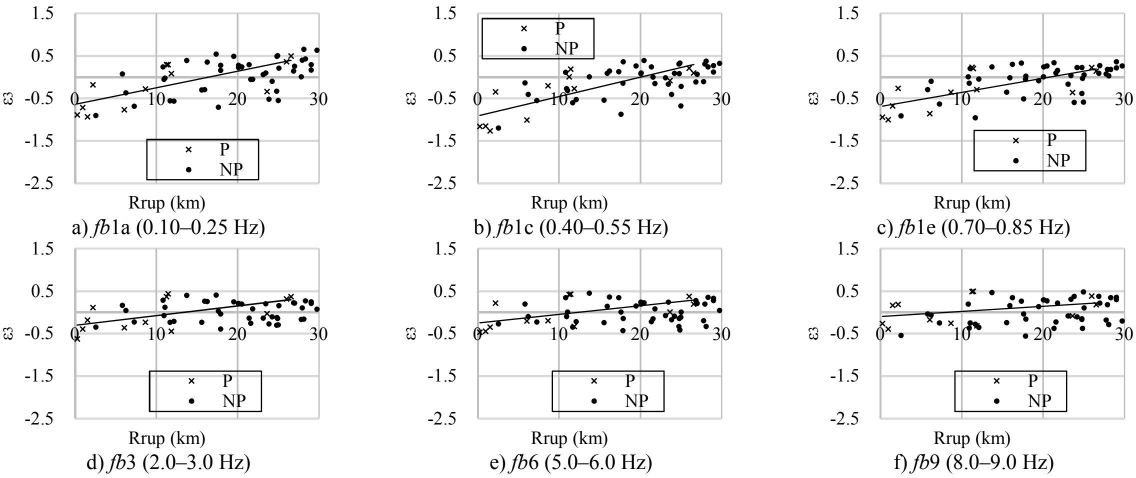

Fig. 8 – Relationships between residual (ε_3) and R_{rup} for $\mu_{tgr,h}$

4. Regression result

The regression coefficients are shown in Figs.9–11 and Table 4. It should be noted that $\sigma_{tgr,v}$ in *fb*1b at TTRH02 (earthquake 1), Lucerne (earthquake 10), and KJMA (earthquake 11) were several times greater than $\sigma_{tgr,v}$ in other frequency bands. Although the outliers were eliminated by the procedure described in section 2.2, there were frequencies where t_{gr} was close to $\mu_{tgr,v}\pm 4\ \sigma_{tgr,v}$ and the Fourier amplitude was small. After these t_{gr} were eliminated, $\mu_{tgr,v}$ and $\sigma_{tgr,v}$ were updated. The decrease of energy was less than 2.1 %. The regression coefficients were computed based on the updated $\mu_{tgr,v}$ and $\sigma_{tgr,v}$.

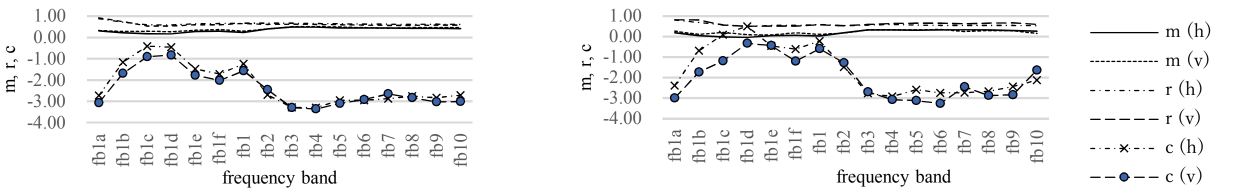

a) For $\mu_{tgr,h}$ and $\mu_{tgr,v}$ b) For $\sigma_{tgr,h}$ and $\sigma_{tgr,v}$

Fig.9 – Regression coefficients (m, r, c) (h: horizontal, v:vertical)

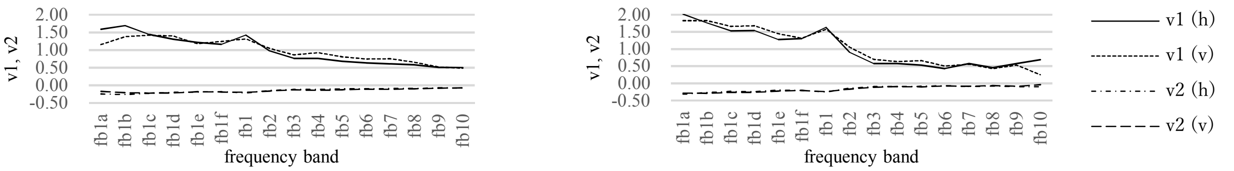

a) For $\mu_{tgr,h}$ and $\mu_{tgr,v}$ b) For $\sigma_{tgr,h}$ and $\sigma_{tgr,v}$

Fig.10 – Regression coefficients (v_1, v_2) (h: horizontal, v:vertical)

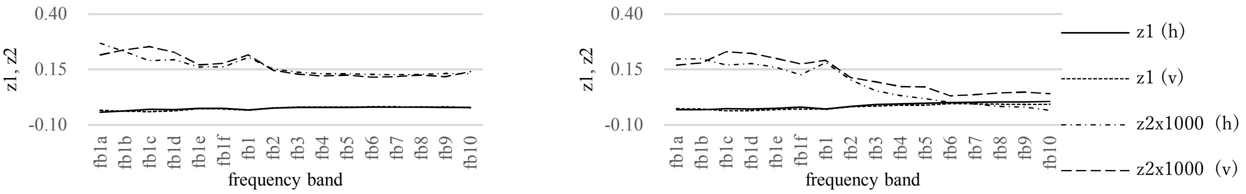

a) For $\mu_{tgr,h}$ and $\mu_{tgr,v}$ b) For $\sigma_{tgr,h}$ and $\sigma_{tgr,v}$

Fig.11 – Regression coefficients (z_1, z_2) (h: horizontal, v:vertical)

Table 3 Regression coefficients relating to directivity effects

	$\mu_{tgr,h}$ (P)			$\sigma_{tgr,h}$ (P)		$\mu_{tgr,h}$ (NP)			$\sigma_{tgr,h}$ (NP)		$\mu_{tgr,v}$			$\sigma_{tgr,v}$	
	d_2	d_3	*S.D.*	d_1	*S.D.*	d_2	d_3	*S.D.*	d_1	*S.D.*	d_2	d_3	*S.D.*	d_1	*S.D.*
fb 1a	0.0389	-0.6379	0.378	0.0322	0.710	0.0238	-0.4415	0.379	0.0061	0.535	0.0320	-0.5688	0.444	0.0179	0.617
fb 1b	0.0478	-0.9591	0.440	0.0495	0.590	0.0229	-0.4387	0.327	0.0009	0.416	0.0348	-0.7172	0.435	0.0242	0.625
fb 1c	0.0455	-0.9110	0.375	0.0472	0.601	0.0286	-0.6243	0.339	0.0101	0.430	0.0467	-0.9346	0.477	0.0271	0.617
fb 1d	0.0381	-0.7567	0.413	0.0468	0.618	0.0168	-0.3780	0.311	0.0102	0.383	0.0408	-0.7866	0.446	0.0295	0.654
fb 1e	0.0331	-0.6881	0.350	0.0391	0.488	0.0186	-0.4099	0.334	0.0137	0.450	0.0343	-0.6366	0.399	0.0261	0.765
fb 1f	0.0375	-0.6458	0.385	0.0323	0.552	0.0070	-0.1901	0.297	0.0086	0.411	0.0168	-0.3279	0.352	0.0096	0.642
fb 1	0.0404	-0.7809	0.374	0.0409	0.465	0.0207	-0.4319	0.292	0.0084	0.350	0.0341	-0.6629	0.377	0.0194	0.487
fb 2	0.0268	-0.4237	0.352	0.0166	0.518	0.0033	-0.0882	0.253	-0.0015	0.358	0.0149	-0.2916	0.282	0.0072	0.405
fb 3	0.0227	-0.3029	0.311	0.0146	0.441	-0.0022	0.0373	0.236	-0.0096	0.350	0.0146	-0.2878	0.276	0.0120	0.403
fb 4	0.0130	-0.1150	0.286	-0.0013	0.507	0.0027	-0.0857	0.266	-0.0066	0.414	0.0085	-0.1781	0.309	0.0017	0.391
fb 5	0.0187	-0.2399	0.294	0.0120	0.459	0.0006	-0.0420	0.252	-0.0113	0.381	0.0103	-0.2001	0.296	0.0046	0.410
fb 6	0.0203	-0.2493	0.296	0.0009	0.310	-0.0020	0.0179	0.243	-0.0150	0.318	0.0076	-0.1454	0.305	0.0002	0.364
fb 7	0.0162	-0.1709	0.312	0.0011	0.459	-0.0015	-0.0113	0.252	-0.0124	0.339	0.0109	-0.2012	0.282	0.0016	0.394
fb 8	0.0145	-0.1257	0.362	-0.0027	0.499	0.0023	-0.0665	0.227	-0.0129	0.366	0.0098	-0.1532	0.289	0.0051	0.446
fb 9	0.0185	-0.1428	0.285	-0.0065	0.365	0.0078	-0.1491	0.259	-0.0048	0.395	0.0147	-0.2368	0.317	0.0041	0.411
fb 10	0.0121	-0.0980	0.313	-0.0042	0.344	0.0146	-0.2688	0.285	-0.0064	0.369	0.0116	-0.1778	0.321	0.0028	0.419

In Fig.9, the regression coefficients for M_w and R_{rup} are presented. Except in *fb*1c and *fb*1d, the values of m are positive for $\sigma_{tgr,h}$. In general, the duration could be long as the increase in the rupture area. Moreover, all values of r are positive.

Fig.10 presents the regression coefficients for V_{s30}. As the frequency increases, the values of v_1 (intercept) and v_2 (slope) approach zero. Additionally, the regression coefficients for $Z_{1.0}$ are shown in Fig.11. In general, the value of z_2 (slope) decreases as the frequency increases. Hence, the effect of soil properties could be more significant in low frequency bands.

For the forward directivity effect, the regression coefficients d_1, d_2, and d_3 are shown in Table 4. The coefficients were computed for the ε_3 data of the ten earthquakes with R_{rup} less than 26.55 km. The values of d_1, d_2, and d_3 for the vertical component were also computed to modify the effect of h. As shown in Table 4, the values of d_1 (slope) for P are larger than those for NP, especially from fb1a to fb1. However, this difference decreases as the frequency increases. A similar tendency can be observed for $\mu_{tgr,h}$. From Table 4, it can be pointed out that the values of d_3 (intercept) for P are less than those of d_3 for NP from fb1a to fb3. Hence, for a small R_{rup}, $\mu_{tgr,h}$ for P tends to be less than $\mu_{tgr,h}$ for NP in low frequency bands.

The standard errors involved when μ_{tgr} and σ_{tgr} are modeled using M_w, R_{rup}, V_{s30}, and $Z_{1.0}$ are presented in Fig.12. The standard errors for σ_{tgr} are greater than the standard errors for μ_{tgr}.

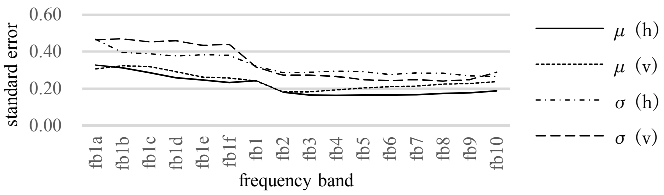

Fig.12 – Standard errors (h: horizontal, v:vertical)

5. Effect of each parameter

5.1 M_w and R_{rup}

The predicted values of $\sigma_{tgr,h}$ for different M_w and R_{rup} are plotted in Fig.13. Fig.13a depicts the tendency of $\sigma_{tgr,h}$ to increase as M_w increases. In addition, the effect of M_w appears to be more prominent in high frequency bands. Fig.13b shows that $\sigma_{tgr,h}$ increases with the increase in $R_{rup}$for all frequency bands.

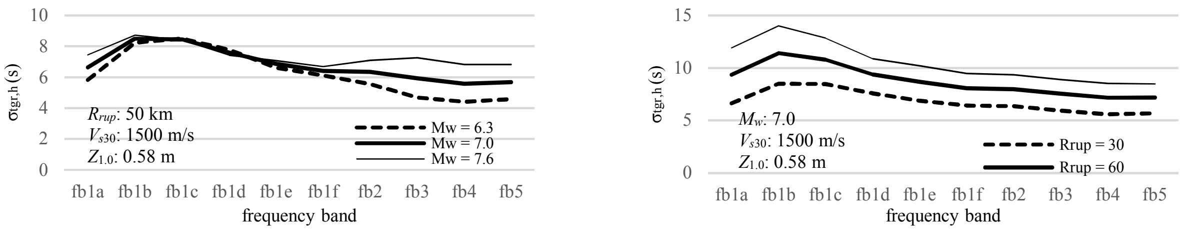

a) Effect of M_w b) Effect of R_{rup}

Fig.13 – Predicted values of $\sigma_{tgr,h}$ for different a) M_w and b) R_{rup}

5.2 V_{s30} and $Z_{1.0}$

The predicted values of $\sigma_{tgr,h}$ based on the three soil classes [16] are presented in Fig.14. The soil properties are listed in Table 4. The values of $Z_{1.0}$ were computed using Eq. (6a). As shown in Fig.14, the predicted $\sigma_{tgr,h}$ for stiffer soils (i.e., soils with a high value of V_{s30}) are larger than those for softer soils in low frequency bands. However, the effect of soil properties virtually disappears in frequencies exceeding 2.0 Hz.

5.3 Forward directivity effect

The predicted values of $\sigma_{tgr,h}$ for P and NP with R_{rup} = 5 km and R_{rup} = 25 km are depicted in Fig.15. As shown in Fig.15a (R_{rup} = 5 km), the ratio of $\sigma_{tgr,h}$ for P and $\sigma_{tgr,h}$ for NP is large in low frequency bands, indicating that the forward directivity effect might be prominent in these low frequency bands. However, the difference between $\sigma_{tgr,h}$ for P and NP was small when R_{rup} = 25 km.

Table 4 V_{s30} and $Z_{1.0}$ for different soil classes

Soil class	V_{s30} (m/s)	$Z_{1.0}$ (m)
A	1500	0.58
C	560	67.8
E	180	742

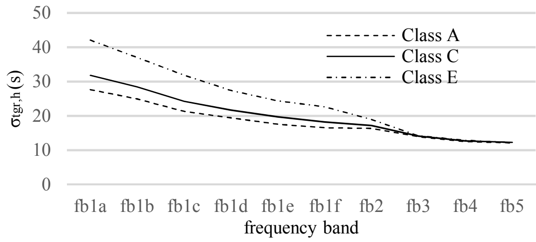

Fig.14 – Predicted values of $\sigma_{tgr,h}$ for different soil classes

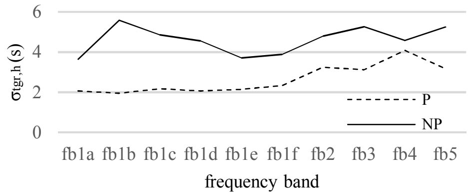

a) R_{rup} = 5 km

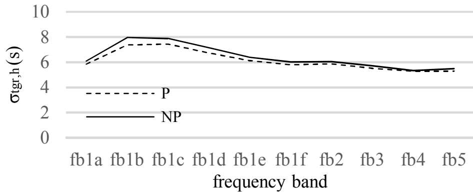

b) R_{rup} = 25 km

Fig.15 – Predicted values of $\sigma_{tgr,h}$ for pulse-like (*P*) and non-pulse-like ground motions (*NP*)

6. Conclusions

The conclusions of this study are as follows:

1. As the moment magnitude or the closest source-to-site-distance increased, the values of the mean and standard deviation of group delay time also tended to increase for all frequency bands.
2. As the lateral stiffness of the ground surface decreased or as the thickness of sedimentary layer increased, the values of the mean and standard deviation of group delay time tended to increase in the low frequency bands.
3. The values of the mean and standard deviation of group delay time for pulse-like ground motions were less than those for other ground motions in low frequency bands. This difference increased as the closest source-to-site-distance decreased.

Acknowledgements

The authors used acceleration records provided by KiK-net and NGA-West2 databases.

References

[1] Ohsaki Y(1979): On the significance of phase content in earthquake ground motions, *Earthquake Engineering and Structural Dynamics*, 7:5, pp.427-439.

[2] Izumi M, Katsukura H(1983): A fundamental study on extraction of phase-information in earthquake motions, *Journal of Structural and Construction Engineering* (*Transaction of AIJ*), Vol.327, pp.20-25. (in Japanese)

[3] Nagao K, Kanda J (2015): S Estimation of Damping Correction Factors Using Duration Defined by the Standard Deviation of Phase Difference, *Earthquake Spectra*, Vol. 31, No. 2, pp.761-783.

[4] Nagao K, Kanda J (2018): Generation Method of Ground Motions Compatible with Design Response Spectra and Energy Spectra in All Frequency Bands, *Structural engineering* (*AIJ*), Vol.64B, pp.81-92.

[5] Novikova EI, Trifunac MD (1994): Duration of strong ground motion in terms of earthquake magnitude, epicentral distance, site conditions, and site geometry, *Earthquake Engineering and Structural Dynamics*, 23:9, pp.1023-1043.

[6] Kempton JJ, Stewart JP (2006): Prediction equations for significant duration of earthquake ground motions considering site and near-source effects, *Earthquake Spectra*, Vol. 22, No. 4, pp.985-1013.

[7] Bommer JJ, Stafford PJ, Alarcon JE (2009): Empirical equations for the prediction of the significant, bracketed, and uniform duration of earthquake ground motion, *Bulletin of Seismological Society of America*, Vol. 99, No. 6, pp.3217-3233,

[8] Nojima N (2015): Development of Empirical Equations for Prediction of Significant Duration of Strong Ground Motions, *Journal of Japan Association for Earthquake Engineering*, Vol.15, No.6, pp.25-43. (in Japanese).

[9] Nagao K, Kanda J (2011): Study on the relationship between outliers of phase differences and Fourier amplitude, *JCOSSAR 2011*. (in Japanese)

[10] Abrahamson NA, Silva WJ, Kamai R (2014): Summary of the ASK14 ground motion relation for active crustal regions, *Earthquake Spectra*, Vol. 30, No. 3, pp.1025-1055.

[11] Boore DM, Stewart JP, Seyhan E, Atkinson GM (2014): NGA-West2 equations for predicting PGA, PGV, and 5% damped PSA for shallow crustal earthquakes, *Earthquake Spectra*, Vol. 30, No. 3, pp.1057-1085.

[12] Chiou BSJ, Youngs RR (2014): Update of the Chiou and Youngs NGA model for the average horizontal component of peak ground motion and response spectra, *Earthquake Spectra*, Vol. 30, No. 3, pp.1117-1153.

[13] Sommerville PG, Smith NF (1996): Accounting for near-fault rupture directivity effects in the development of design ground motions, Proceeding of 11th World Conference on Earthquake Engineering, Paper No. 711.

[14] Shahi SK, Baker JW (2013): A probabilistic framework to include the effects of near-fault directivity in seismic hazard assessment, *Report No.180*, The John A. Blume Earthquake Engineering Center, Stanford, USA.

[15] Hayden CP (2014): Liquefaction-induced building performance and near-fault ground motions, ph.D. thesis, University of California, Berkeley, USA.

[16] Building Seismic Safety Council (2004): NEHRP Recommended Provisions for Seismic Regulations for New Buildings and Other Structures (FEMA 450), 2003 edition, National Institute of Building Sciences, Washington, DC, USA.

